JOURNAL OF CHEMICAL & ENGINEERING DATA

Article

pubs.acs.org/jced

Experimental and Theoretical Insight of Nonisothermal Adsorption Kinetics for a Single Component Adsorbent–Adsorbate System

Wai Soong Loh,[†] Anutosh Chakraborty,[‡] Bidyut Baran Saha,[§] and Kim Choon Ng*[,†]

[†]Department of Mechanical Engineering, National University of Singapore, 9 Engineering Drive 1, Block EA, 07-08, Singapore 117576

[‡]School of Mechanical and Aerospace Engineering, Nanyang Technological University, 50 Nanyang Avenue, Singapore 639798

[§]Department of Mechanical Engineering, Kyushu University, 744 Motooka, Nishi-ku, Fukuoka 819-0395, Japan

ABSTRACT: A theoretical framework is proposed to describe the temperature-dependent adsorption kinetics and their interpretation of measured uptake curves of four types of adsorbate, namely, methane and halogenated refrigerants (R134a, R410a, and R507a) onto a pitch-based activated carbon, Maxsorb III. The model requires only two measurable data from the experiments, that is, the adsorbent temperature and system pressure during the adsorption dynamics. We have demonstrated that the temperature dependency adsorption has significant influence on the intrapellet diffusion coefficients of the linear driving force (LDF) model. A modified LDF model is proposed in this paper, and it is validated using the uptake behavior of these adsorbates; good agreement is found between the proposed kinetics model and the experimental uptake. The parameters postulated in the model are consistent and reproducible and agree well with a priori estimates. The model provides a useful theoretical basis for the analysis of rapid sorption processes for which the isothermal approximation is no longer valid.

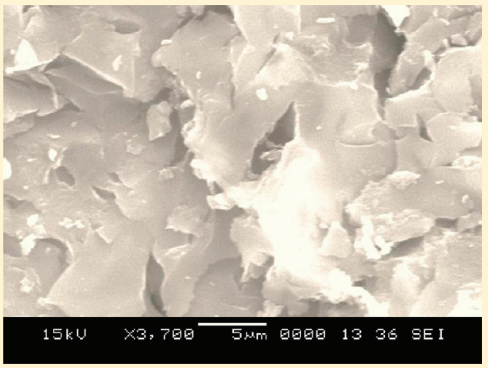

INTRODUCTION

In adsorption systems, the equilibrium adsorption capacity of an adsorbent–adsorbate pair takes a relatively long time period to reach an equilibrium state. For practical consideration, temperature transients owing to the isosteric heat of adsorption during an adsorption uptake are equally important for the estimation of sorption capacity, particularly in designing cyclic processes. The existing adsorption kinetics models found in the literature, worked well with equilibrium conditions, but they are inaccurate in predicting the vapor uptake associated with rapid temperature transients of adsorption or desorption processes. Therefore, it is necessary to develop a theoretical kinetic model as well as to have such models verified with adsorption kinetics experiments.

Since the 1950s, the linear driving force (LDF) model has been proposed by Glueckauf,[1] Gullieminot et al.,[2] and Lathan and Burgess.[3] A useful mathematical framework for the LDF was further deliberated by Sircar and Hufton[4] and Li and Yang[5] where the equilibrium adsorption concentration profile was maintained in activated carbon with a gas-phase adsorbate. Fletcher et al.[6,7] conducted experiments on the adsorption kinetics of *n*-octane, *n*-nonane, methanol, and benzene on type BAX 950 activated carbon, and they correlated the LDF model to their kinetic data. Similar kinetics experiments for hydrocarbon onto activated carbon and silica gel had been performed by Malek and Farooq,[8] whereas Scholl et al.[9] conducted kinetics experiments for water vapor, *n*-hexane, cyclohexane, and tetrachloroethylene on single pellets of activated carbon. In recent years, El-Sharkawy et al.[10] and Saha et al.[11] also reported the adsorption kinetics of ethanol on activated carbon fiber using the LDF model. Reid and Thomas[12,13] studied the adsorption of gases on molecular sieves carbon (MSC), and they reported that the adsorption kinetics followed a similar trend described by LDF. Harding et al.[14] found that the LDF model can be used to represent accurately the adsorption of water vapor by activated carbon in a pollutant separation process. These studies employed adsorption processes such as breakthrough behavior, air separation, moving bed systems, pressure swing adsorption, and thermal swing adsorption refrigeration utilizing activated carbon. The point to note is that these experiments were based on the assumption of isothermal adsorption, that is, almost no temperature changes to the adsorbent during the adsorption process. The assumption is valid because the sorption samples used were small and the heat released rate is relatively low compared with the heat transfer rate. Although the adsorbate concentration was adjusted at each step change, the difference in adsorbate concentration before and after the initial and equilibrium states was usually negligible, minimizing the temperature excursion. However, some studies have noted a significant discrepancy in diffusivities of adsorbent–adsorbate pairs even though they were at similar isotherms,[15−17] and these have been attributed to temperature effects.

For a rapid diffusing system, the sorption kinetics is influenced by the thermal excursion effects, as reported by Eagan et al.,[18]

Received: November 13, 2011
Accepted: March 1, 2012
Published: April 2, 2012

Doelle and Riekert,[19] Ilavský et al.,[20] and Voloshchuk et al.[21−23] They have investigated the behavior of zeolite systems. The nonisothermal adsorption kinetics of *n*-butane on extruded cylindrical activated carbon and dichloromethane on activated carbon were also investigated by Fiani et al.[24] and Meunier et al.,[25] respectively. Most studies reported a rapid temperature rise, and the uptake curves showed significant deviation from the predictions of isothermal systems.

Despite the available nonisothermal models for adsorbate diffusivity of adsorbent−adsorbate pairs[26−37] covering many refrigerants and hydrocarbons, they were merely based on semiempirical models. The detailed approaches, such the Fickian diffusion models, involved mainly the mass-transfer mechanism which tended to be complicated and time-consuming when the thermal effects were incorporated into the adsorbate diffusivity. The motivation of the present paper is to develop a thermodynamic framework to account for both pressure and temperature excursions during rapid uptake or off-take of adsorbate from the porous adsorbents.

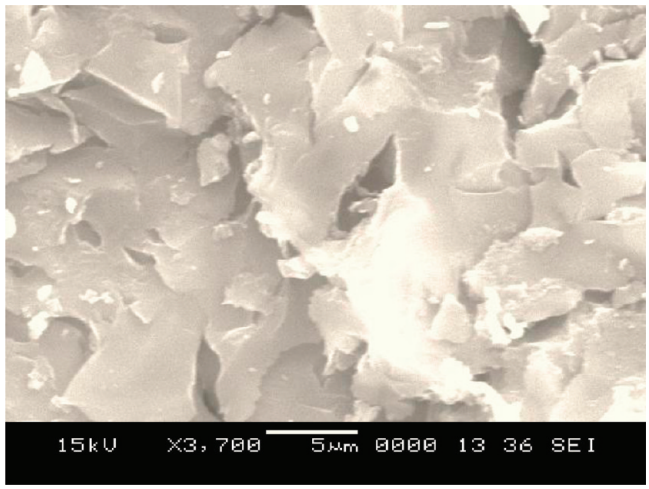

Figure 1. Scanning electron micrograph (SEM) of Maxsorb III activated carbon at 3700 magnification.

THEORY

Isothermal Adsorption Kinetics. The LDF model is a simple and yet widely used kinetic equation for adsorbent−adsorbate uptake in an isothermal condition. The intrapellet diffusion behavior is accounted for by the overall mass diffusion coefficient ($k_s a_v$), and the rate of uptake is proportional to the difference between the equilibrium uptake, q^*, and the instantaneous uptake, $q(t)$, as follows,

$$\frac{d\bar{q}}{dt} = k_s a_v[q^* - q(t)] \tag{1}$$

It is also noted that $k_s a_v$ is also a function of adsorbate concentration. This correlation is valid for isothermal adsorption, where the temperature change of the adsorbent is neglected during the adsorption process when the concentration difference between the initial and the equilibrium adsorption is small and the heat transfer rate is negligible. For rapid diffusing systems, the sorption kinetics may be appreciably influenced by the thermal effects.

Nonisothermal Adsorption Kinetics. The significance of thermal effects in the zeolite systems and adsorption kinetics of *n*-butane on extruded cylindrical activated carbon has been demonstrated experimentally,[18,19,24] and the uptake curves showed significant deviation from that of isothermal systems. The adsorbate diffusivities of solid adsorbents from nonisothermal uptake data were measured in a gravimetric or in a volumetric apparatus[16,26−28,31−36] and the thermal effects, and the effect of pressure onto the adsorption rate was reported by He et al.[37]

With these, the present study was therefore undertaken to provide a comprehensive theoretical framework for the investigation of thermal and pressure effects in adsorption measurements. A modified linear-driving-force (mLDF) model based on the adsorbent temperature and system concentration is developed to interpret experimental adsorption uptake curves. Furthermore, the sudden change of adsorbate concentration during the initial stage of adsorption processes is also incorporated into the kinetics model.

From mathematics, the total derivative of the instantaneous uptake can be expressed from the partial contributions of pressure and temperature using the chain rule as represented by eq 2.

$$\frac{d\bar{q}}{dt}(P, T) = \left.\frac{\partial \bar{q}}{\partial P}\right|_T \frac{dP}{dt} + \left.\frac{\partial \bar{q}}{\partial T}\right|_P \frac{dT}{dt} \tag{2}$$

The first term on the right-hand side is the partial derivative of the instantaneous uptake with respect to system pressure at constant temperature. The second term shows the partial derivative of instantaneous uptake with respect to temperature at constant pressure. The details of the partial derivatives are presented in the following equations, by which the effects of adsorbent temperature and system pressure are integrated. The

$$\left.\frac{\partial \bar{q}}{\partial P}\right|_T \frac{dP}{dt} = k_s a_v[q^* - q(t)]\left\{1 + \left[1 - \exp\left(\frac{-3P(t)}{2P^*}\right)\right]\right\} \tag{3}$$

$$\left.\frac{\partial \bar{q}}{\partial T}\right|_P \frac{dT}{dt} = \beta[q^* - q(t)]\left\{1 - \frac{T^*}{T(t)}\right\} \tag{4}$$

P^* and T^* in eqs 3 and 4 represent the equilibrium pressure and temperature, respectively. Similarly $P(t)$ and $T(t)$ represent the instantaneous process pressures and adsorbent temperatures when adsorption takes place. $k_s a_v$ and β are the effective mass transfer coefficient corresponded to the process equilibrium pressures and temperatures, respectively, that is, $k_s a_v(P^*)$, $\beta(T^*)$. Both $k_s a_v$ and β are measured in s^{-1}. The second term on the right-hand side of eq 3 represents the unit-step function for the system pressures profile, which enable the prediction of the system pressures during adsorption. The corresponding second term on the right-hand side in eq 4 represents the adsorbent temperature profile, which enable the estimation of the system temperature.

Substituting eqs 3 and 4 into eq 2 results in:

$$\frac{d\bar{q}}{dt}(P, T) = \alpha[q^* - q(t)] \tag{5}$$

dx.doi.org/10.1021/je201210t | J. Chem. Eng. Data 2012, 57, 1174−1185

where α is the overall effective mass transfer coefficient and is presented below as

$$\alpha = k_s a_v \left\{1 + \left[1 - \exp\left(\frac{-3P(t)}{2P^*}\right)\right]\right\} + \beta\left\{1 - \frac{T^*}{T(t)}\right\} \quad (6)$$

The effective mass transfer coefficient, $k_s a_v$, can be expressed as the function of the surface diffusion as given by eq 7 as,[1]

$$k_s a_v = \frac{F_o D_s}{R_p^2} \quad (7)$$

Table 1. Porous Characteristics of Maxsorb III

	BET surface areas	micropore volume	average pore diameter	skeletal density
adsorbent	$m^2 \cdot g^{-1}$	$cm^3 \cdot g^{-1}$	nm	$g \cdot cm^{-3}$
Maxsorb III	3150	1.7	2	2.2

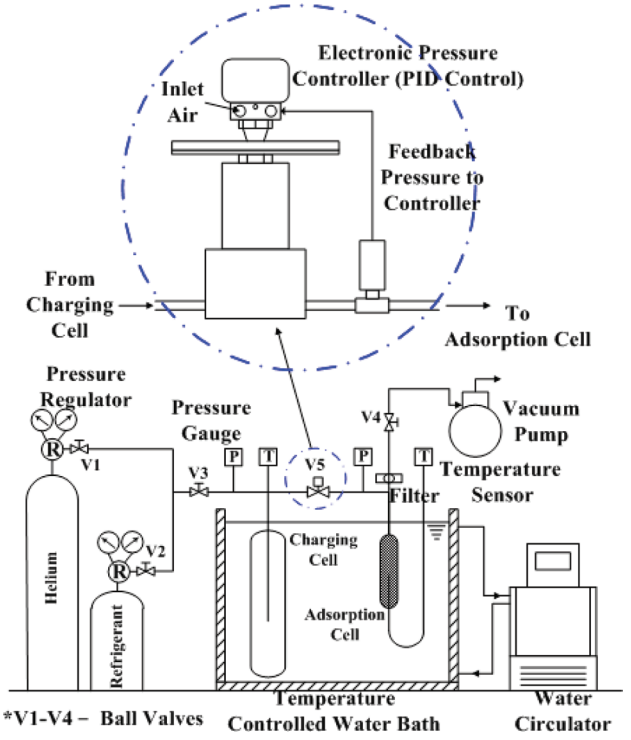

Figure 2. Schematic of the volumetric adsorption kinetics experimental apparatus.

where F_o is a constant, D_s is the surface diffusion ($m^2 \cdot s^{-1}$), and R_p is the particle radius (m).

The relation between the surface diffusion and adsorption temperature can be given by the Arrhenius form as

$$D_s = D_{so} \exp\left(\frac{-E}{RT}\right) \quad (8)$$

where E is the activation energy of the adsorbate ($J \cdot kg^{-1}$). D_{so} is a pre-exponential constant that varies with the equilibrium pressure. By applying eq 8 into eq 7, the effective mass transfer coefficient, $k_s a_v$ can be expressed as

$$k_s a_v = D^*_{so} \exp\left(\frac{-E}{RT}\right) \quad (9)$$

where

$$D^*_{so} = \frac{F_o D_{so}}{R_p^2}$$

is a function of equilibrium pressure, P^*.

The correlations for $k_s a_v$ and β are present in eqs 10 and 11, respectively, as

$$k_s a_v = \left[A_1\left(\frac{P^*}{P_{cri}}\right) + A_2\right] \exp\left(\frac{-E}{RT}\right) \quad (10)$$

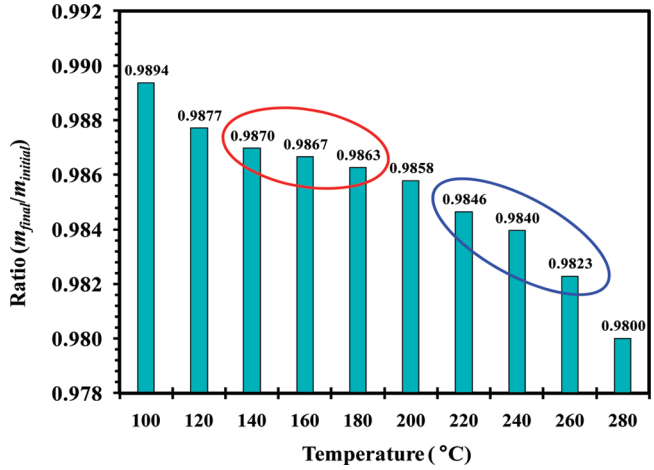

Figure 4. Ratios of final mass and initial mass of the Maxsorb III activated carbon sample at different regeneration temperatures.

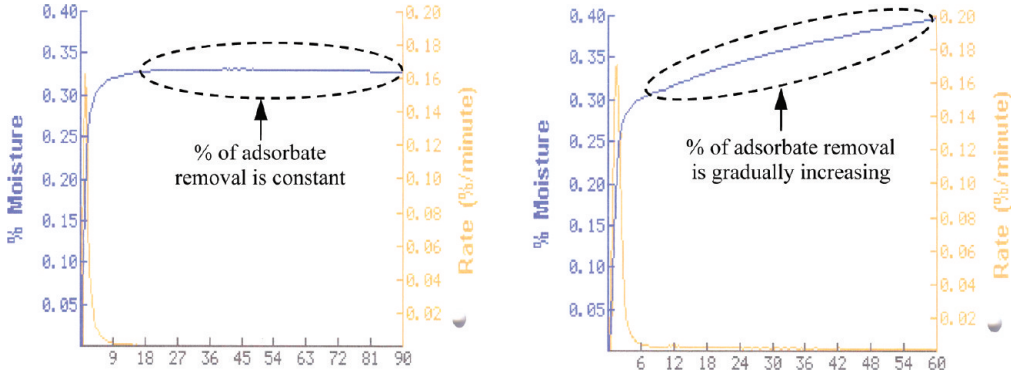

Figure 3. Percentage and the rate of moisture removal as a function of time.

dx.doi.org/10.1021/je201210t | J. Chem. Eng. Data 2012, 57, 1174–1185

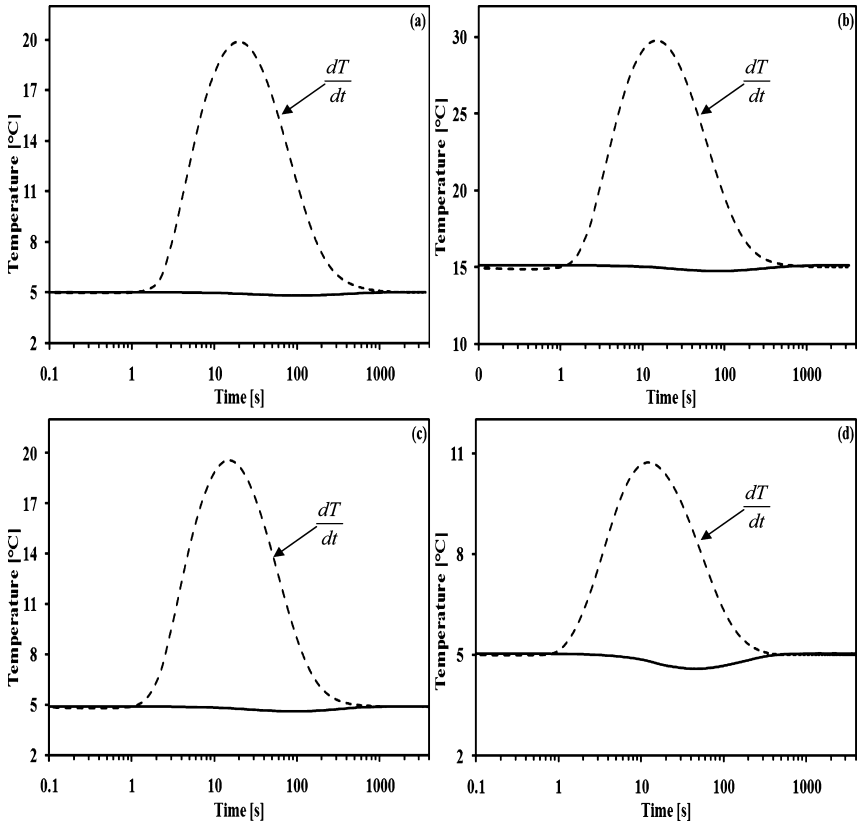

Figure 5. Charging cell (—) and adsorbent (- - -) temperature versus time during adsorption kinetics process for (a) Maxsorb III-R134a at P^* = 3.1 bar, T^* = 5 °C, (b) Maxsorb III-R410a at P^* = 6.3 bar, T^* = 15 °C, (c) Maxsorb III-R507a at P^* = 6.1 bar, T^* = 5 °C, and (d) Maxsorb III-CH_4 at P^* = 9.1 bar, T^* = 5 °C.

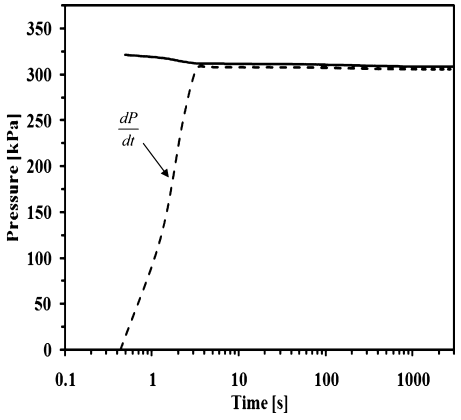

Figure 6. Charging cell (—) and adsorption cell (- - -) pressure versus time during adsorption kinetics process for Maxsorb III-R134a at P^* = 3.1 bar, T^* = 5 °C.

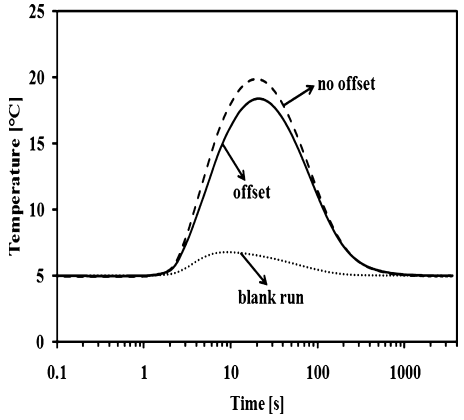

Figure 7. Adsorption cell temperature during the kinetics process for Maxsorb III-R134a at P^* = 3.1 bar, T^* = 5 °C.

$$\beta = \exp\left[B_1\left(\frac{T^*}{T_{cri}}\right) + B_2\right] \tag{11}$$

In logarithmic form, eq 11 may be written as

$$\ln(\beta) = B_1\left(\frac{T^*}{T_{cri}}\right) + B_2 \tag{12}$$

where A_1, A_2, B_1, and B_2 are the constant coefficients which can be regressed from the experimental adsorption kinetics data.

If the effects of pressure and temperature are insignificant, eq 5 is reduced to the original LDF model.

$$\frac{d\bar{q}}{dt}(P, T) = \left\{k_s a_v\left[1 + \left(1 - \exp\left(\frac{-3P(t)}{2P^*}\right)\right)\right] + \beta\left[1 + \frac{T^*}{T(t)}\right]\right\}[q^* - q(t)] \approx k_s a_v[q^* - q(t)]$$

dx.doi.org/10.1021/je201210t | J. Chem. Eng. Data 2012, 57, 1174−1185

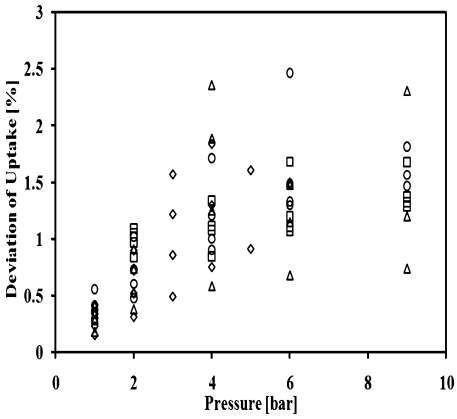

Figure 8. Deviation of uptake capacity between kinetics test with and without temperature offset for ◊, R134a; ○, R410A; △, R507a and □, methane at temperatures range from (5 to 45) °C.

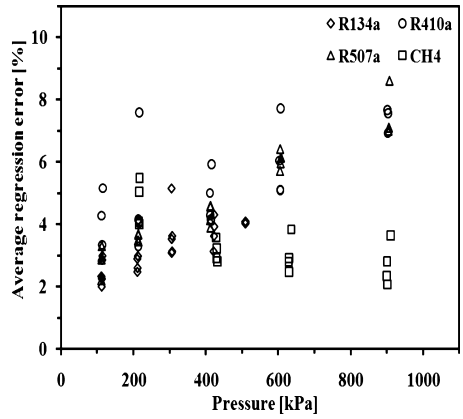

Figure 10. Average regression errors between nonisothermal kinetics model and experimental uptake for ◊, R134a; ○, R410A; △, R507a and □, methane with activated carbon Maxsorb III.

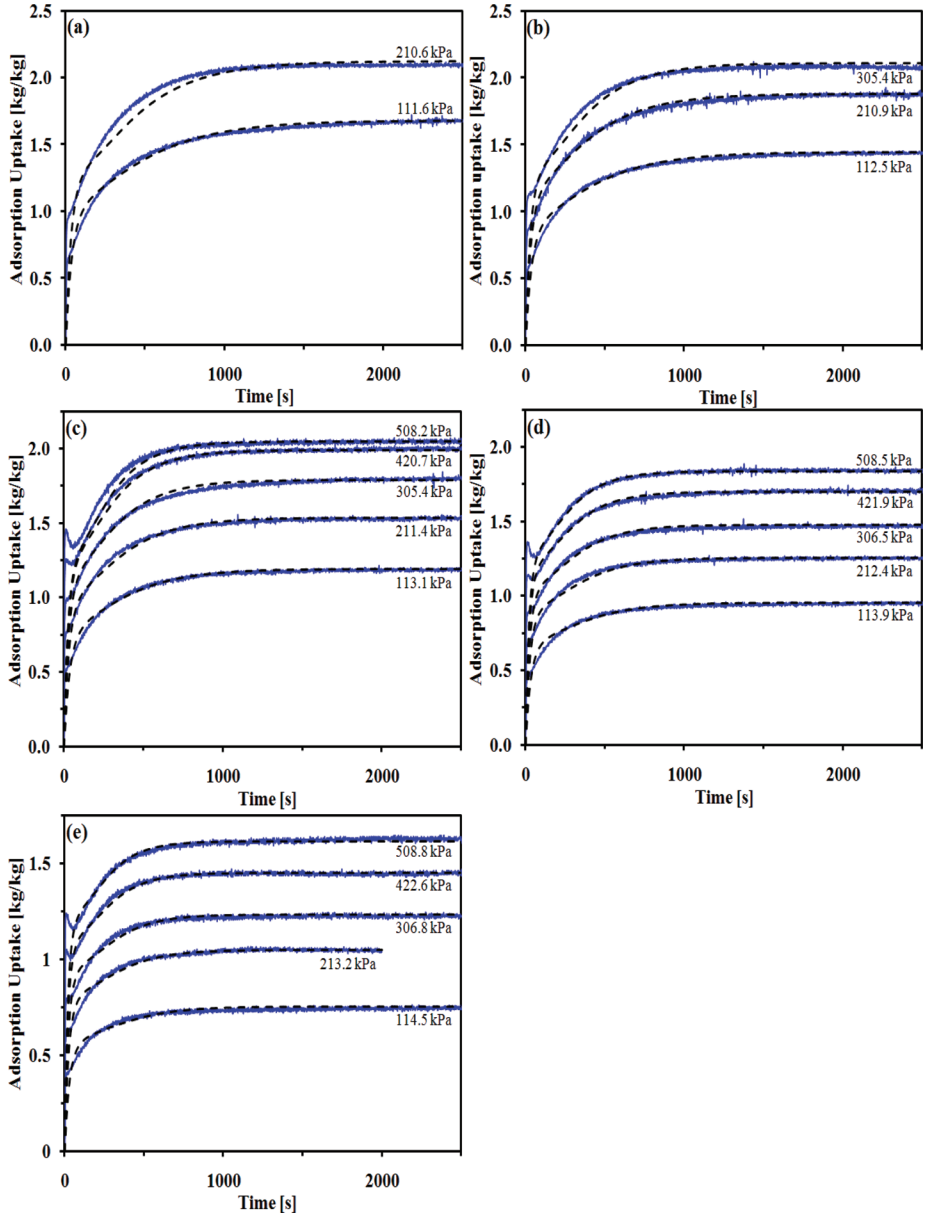

Figure 9. Experimental (—) and predicted (- - -) adsorption uptake for Maxsorb III-R134a versus time at various pressures under adsorption temperature of (a) 5 °C, (b) 15 °C, (c) 30 °C, (d) 45 °C, and (e) 60 °C.

dx.doi.org/10.1021/je201210t | J. Chem. Eng. Data 2012, 57, 1174–1185

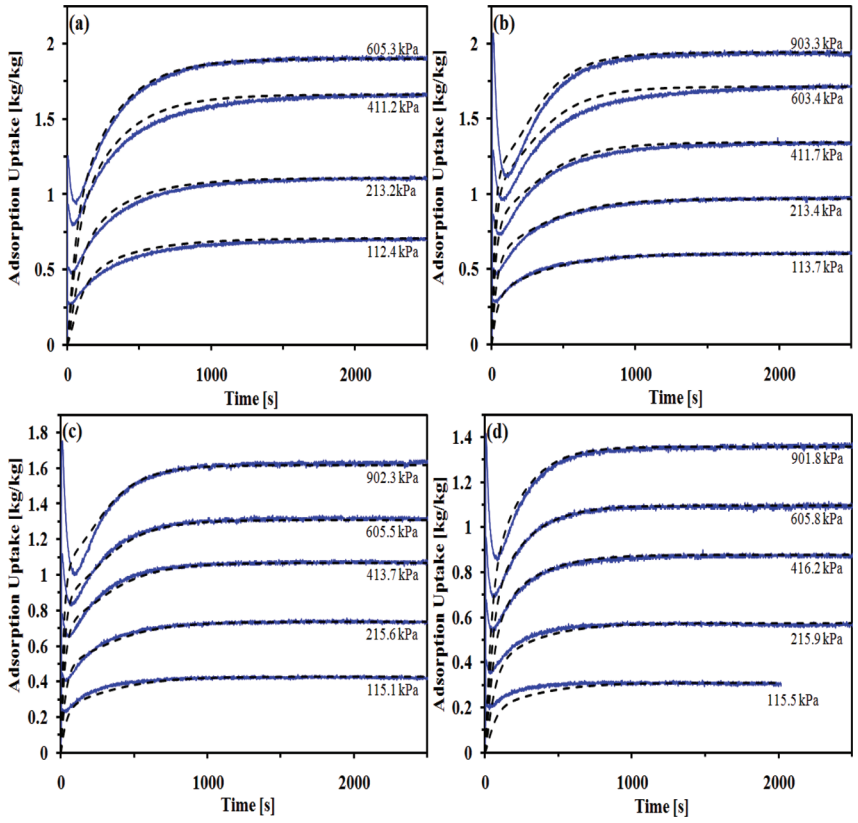

Figure 11. Experimental (—) and predicted (- - -) adsorption uptake for Maxsorb III-R410a versus time at various pressures and adsorption temperature of (a) 5 °C, (b) 15 °C, (c) 30 °C, and (d) 45 °C.

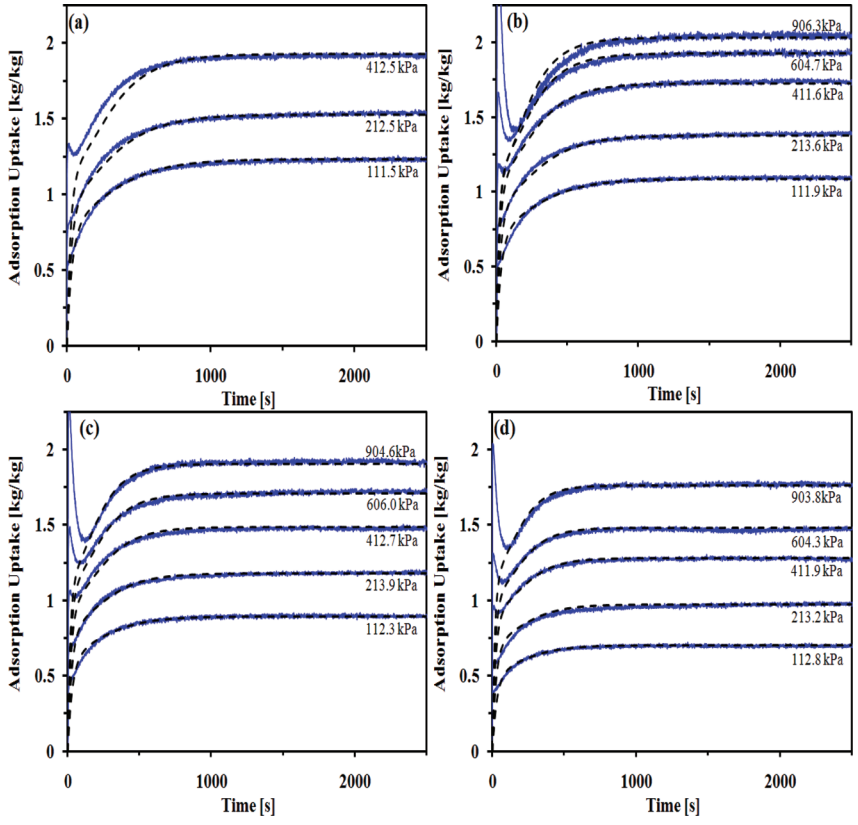

Figure 12. Experimental (—) and predicted (- - -) adsorption uptake for Maxsorb III-R507a versus time at various pressures and adsorption temperature of (a) 5 °C, (b) 15 °C, (c) 30 °C, and (d) 45 °C.

dx.doi.org/10.1021/je201210t | *J. Chem. Eng. Data* 2012, 57, 1174–1185

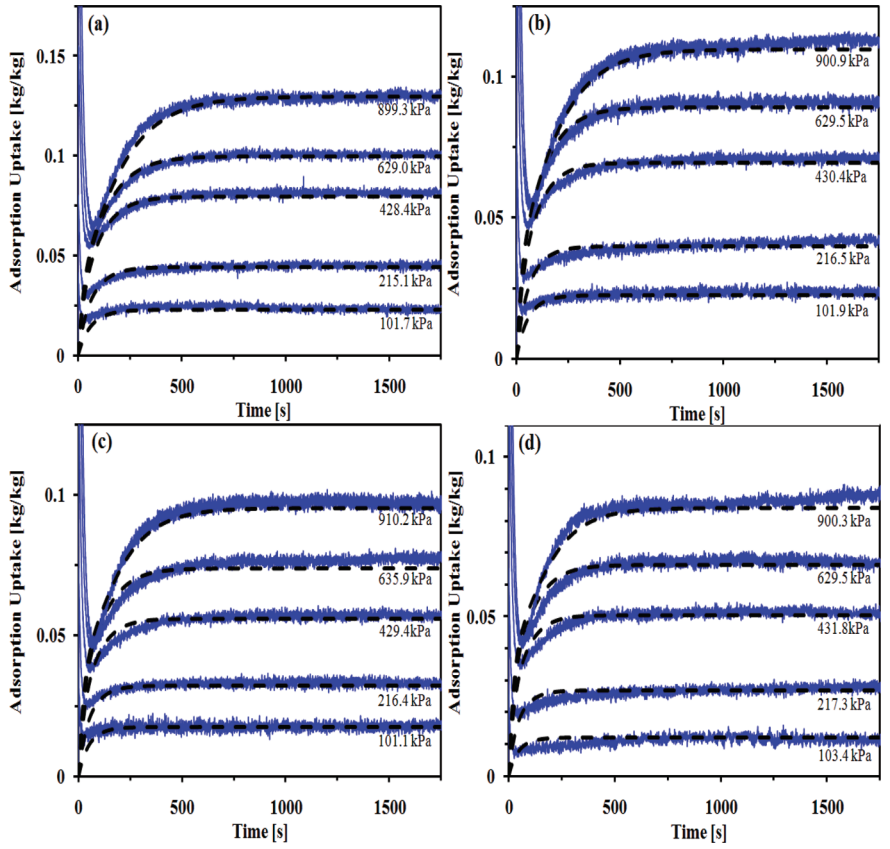

Figure 13. Experimental (—) and predicted (- - -) adsorption uptake for Maxsorb III-methane versus time at various pressures and adsorption temperature of (a) 5 °C, (b) 15 °C, (c) 30 °C, and (d) 45 °C.

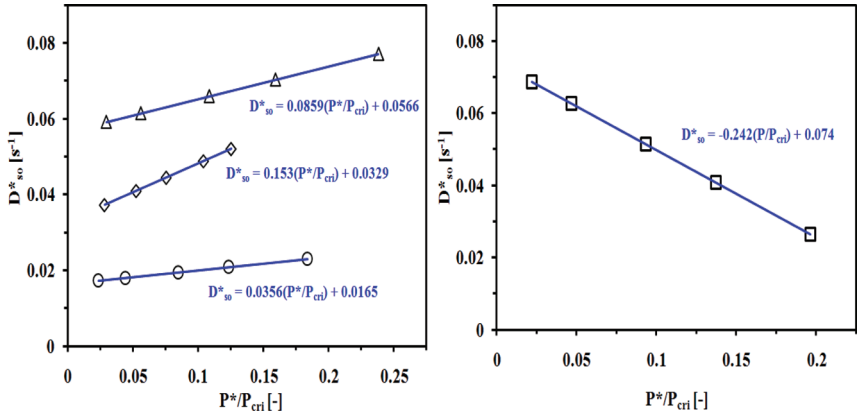

Figure 14. Pressure-dependent pre-exponential constant D^*_{so} plotted against the pressure ratio, P^*/P_{cri} (i.e., eq 11), for ◊, R134a; ○, R410A; △, R507a, and □, methane with activated carbon Maxsorb III.

To determine the instantaneous uptake for a particular adsorbent−adsorbate pair, eq 5 can be rearranged as

$$\frac{d\bar{q}}{q^* - q(t)} = \alpha dt \tag{13}$$

By integrating both sides of eq 13

$$\int \frac{d\bar{q}}{q^* - q(t)} = \int \alpha dt$$

Table 2. Coefficients of the Pre-exponential Function, D^*_{so}, and Temperature Dependence Mass Transfer Coefficient, β

adsorbent	Maxsorb III			
adsorbate	R134a	R410a	R507a	CH_4
P_{cri}/kPa	4059.28	4902.6	3792.1	4599.2
T_{cri}/K	374.21	344.74	343.77	190.65
A_1	0.0859	0.153	0.0356	−0.242
A_2	0.0566	0.0329	0.0165	0.074
B_1	9.14	8.99	7.45	5.25
B_2	−8.3	−8.54	−7.25	−8.85

dx.doi.org/10.1021/je201210t | J. Chem. Eng. Data 2012, 57, 1174−1185

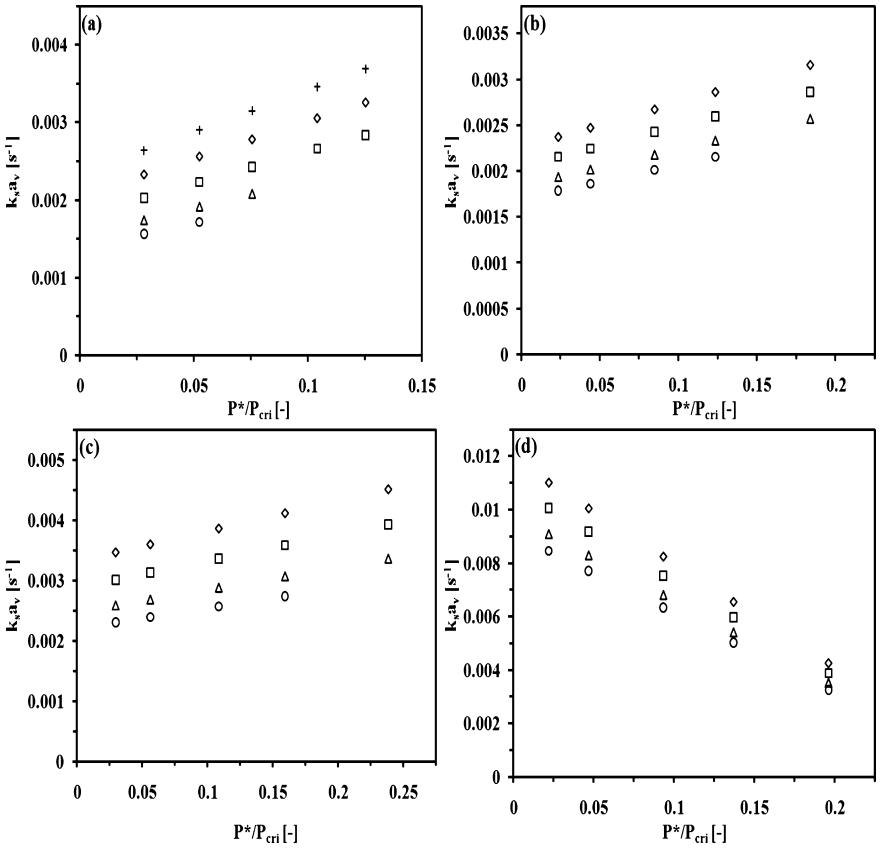

Figure 15. Pressure dependent effective mass transfer coefficient, $k_s a_v$, plotted against pressure ratio, P^*/P_{cri} (i.e., eq 10), for (a) R134a, (b) R410a, (c) R507a, and (d) methane with activated carbon Maxsorb III at adsorption temperature of ○, 5 °C; △, 15 °C; □, 30 °C; ◊, 45 °C, and +, 60 °C.

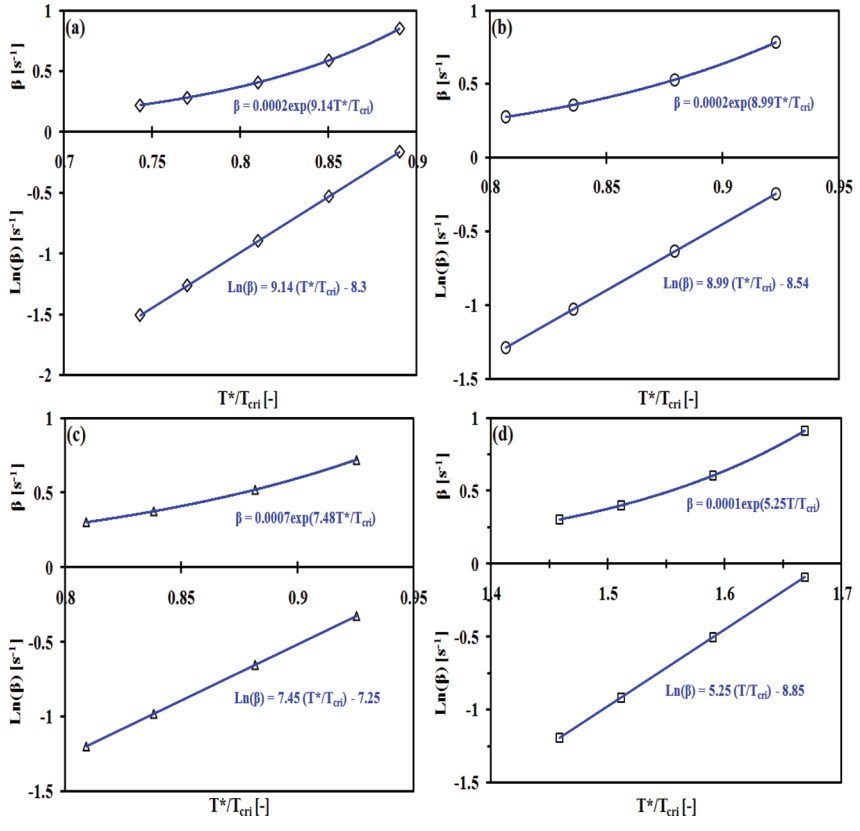

Figure 16. Temperature-dependent effective mass transfer coefficient, β, plotted against temperature ratio, T^*/T (i.e., eq 13), for (a) ◊, R134a; (b) ○, R410A; (c) △, R507a, and (d) □, methane with activated carbon Maxsorb III.

dx.doi.org/10.1021/je201210t | J. Chem. Eng. Data 2012, 57, 1174−1185

$$-\ln[q^* - q(t)] = \alpha t + \text{constant}$$

with initial condition $t = 0$ and $q(t) = 0$, one can get

$$\text{constant} = -\ln(q^*)$$

which implies that

$$\frac{q^* - q(t)}{q^*} = \exp(-\alpha t) \tag{14}$$

Rearranging eq 14, the instantaneous uptake may be expressed as

$$q(t) = q^*[1 - \exp(-\alpha t)] \tag{15}$$

The instantaneous uptake (eq 15) can be employed to predict the experimental adsorption kinetics curves.

EXPERIMENTAL SECTION

The understanding of the transport mechanism of the adsorbent−adsorbate system is crucial in designing the thermally driven sorption system. Extensive studies regarding the adsorbate diffusivity in solid adsorbents using the gravimetric or volumetric apparatus have been conducted previously.[16,18,19,24,26−28,31−35,37] Although the indirect volumetric measurement method is likely to be less accurate, Belmabkhout et al. have shown that the average deviation between these methods is only about 3 %.[38] Hence, the volumetric method (constant-volume−variable-pressure, CVVP apparatus) is used to conduct the kinetics test. The present section reports on the experimental adsorption kinetics data for activated carbon, Maxsorb III with methane, R134a, R410a, and R507a for pressures up to 1 MPa and temperatures from (5 to 45) °C.

Materials. Four types of adsorbate, namely, methane, R134a, R410a, and R507a, are used in the kinetics experiment. The Maxsorb III pitch-based activated carbon, which was supplied by Kansai Coke and Chemicals Co. Ltd., Osaka, Japan, is highly microporous and in powder form. The scanning electron microscope (SEM) photograph of Maxsorb III is shown in Figure 1 where the surface structure is observed to be flake-like layers with porous volumes entrenched in between. The thermophysical properties were measured with Autosorb 1-MP machine using N_2 adsorption isotherms at −195.85 °C; the Brunauer−Emmett−Teller (BET) surface area and the specific pore volume are tabulated in Table 1.

Apparatus and Procedure. The experimental apparatus consists mainly of a stainless steel (SS 304) adsorption cell and a charging cell with internal volume of 50 ± 5 % mL and 1000 ± 5 % mL, respectively, at which the schematic for the adsorption and charging chambers where the adsorption process took place in situ are shown in Figure 2. The pneumatically actuated pressure regulator was installed in between the stainless steel adsorption and charging cells through 1/4 in. nominal stainless steel tubing, and a set of compression fittings to withstand pressure of greater than 2 MPa was used. An electronic pressure controller (Emerson-Tescom ER3000) was mounted over the pneumatic actuated regulator which is able to control pressures ranges from subatmosphere to 20 000 psi with flow coefficient up to 45. The resistance of gas flow through the regulator was neglected. The ER3000 is a microcontroller-based device that implements a digital PID (proportional/integral/derivative) control algorithm to regulate process pressure.

Before the adsorbent samples were loaded into the adsorption cell, Maxsorb III was first weighted in the Computrac Max 5000 moisture analyzer, which has an accuracy of ± 0.1 mg. The samples were then heated in situ at 155 °C for 2 h for thorough degasification. The dry masses were recorded as 1000.0 mg. To obtain the optimal regeneration temperature, the activated carbon samples was heated at different temperatures ranging from (110 to 300) °C, and the adsorbate removal rates are recorded as a function of time. Figure 3 provides typical plots for the percentage of adsorbate removed and the removal rate at temperatures (160 and 200) °C, respectively, for the activated carbon sample type Maxsorb III. In these plots, the "% moisture" of the vertical axis should be considered as the percentage of moisture removal. It can be seen that the percentage of moisture removal from the activated carbon became steady after about 20 min of heating at temperature 160 °C, whereas it is gradually increasing in case of temperature at 200 °C. These observations confirm that there is no significant moisture removal in the extended period of heating at 160 °C. However, the gradual percentage moisture increase in case of heating at 200 °C was not exactly due to the moisture removal; rather it is because of the burn off of the activated carbon sample.

Figure 4 shows the bar plot for the ratio of final mass and initial mass of the Maxsorb III sample at different temperatures. It can be seen that the ratios change sharply below 120 °C and they are very close (indicated by red circle) for the temperatures (140 to 180) °C. Again, the sharp changes in ratios (indicated by blue circle) are observed for temperatures above 200 °C which indicates the possibility of burnout of the AC sample at higher temperatures above 200 °C. Therefore, the regeneration temperature is estimated at temperatures of (140 to 160) °C for the activated carbon samples.

In a typical application, the supply pressure was charged into the ER3000 via a pulse-width modulated solenoid valve at the inlet port, and the regulator dome was loaded. The ER3000 detected the pressure from a pressure transducer mounted downstream in the process and compared the feedback signal to the set pressure every 25 ms. If the feedback is lower than the set point, the ER3000 will open its inlet valve, allowing pressure to flow onto the dome of a pressure-reducing regulator. This will open the main valve of the regulator, increasing the downstream pressure. The ER3000 will continue to increase pressure on the dome of the regulator, that is, increasing the downstream pressure until the feedback signal is equal to the set pressure and vice versa.

Apart from this, two pressure transducers (Kyowa-PGS-50KA) were installed at the charging and adsorption cells with a full scale uncertainty of 0.1 % in measurement. The temperatures of the adsorption and charging cells were recorded using class-A Pt 100 Ω RTDs with an estimated uncertainty of ± 0.15 °C. The adsorption cell RTD was in contact with the activated carbon to enable direct temperature measurement. All of the temperature and pressure readings were logged into the Agilent data logger every 1 s to enable real time monitoring of the adsorption uptake.

Prior to the kinetics experiment, the entire assembly was evacuated for 24 h to a vacuum level of 0.5 mbar and degassed at (140 to 160) °C. This temperature range was selected for the optimum degassing of the adsorbent loaded in the adsorption cell. In addition, helium was purged into the system intermittently during regeneration to enhance the residue gas removal.

After evacuation, the adsorption cells were isolated from the charging cell (with valves 3, 4, and 5 closed). The sample was then cooled down to the required adsorption temperature, at which both the adsorption and charging cells were immersed in

a temperature-controlled water bath, which was connected to the heating/refrigeration circulator (HAAKE F8-C35) to maintain the preset temperature within an accuracy of ± 0.01 °C.

When the system stabilized, the charging cell was pressurized with the adsorbate from its source (with valves 4 and 5 closed). After sufficient time for the system to stabilize, the electronic controller was triggered to actuate the pressure regulator. The adsorbate vapor was released into the adsorption cell keeping the pressure constant at a preset value. The pressure and temperature were recorded at 1 s intervals over the entire experiment. A class-A Pt 100 Ω RTD was inserted into the adsorption cell to measure the adsorbent temperature in situ. With this, the adsorbent temperature increases during the adsorption process can be captured. These two readings (system pressure and adsorbent temperature) play the important role in determining the amount of gas adsorbed by the adsorbent. The adsorption process usually takes one hour to reach the equilibrium state.

After each adsorption process, the regulator (V5) was closed to isolate the sorption cell with the charging cell. The adsorbent in the sorption cell was then regenerated at (140 to 150) °C for 8 h, and helium was purged into the system to enhance the removal of residual gas. The adsorption cell was then ready for the next pressure reading. Measurements were made over different quantities of adsorbate in the charging cell to cover a pressure range below the saturation pressure for respective adsorbent, up to 1 MPa. This precaution was necessary to avoid the possibility of condensation of refrigerant in the capillary and the associated errors in the estimation of adsorbate present in the apparatus. The same procedures were repeated for four types of adsorbate, namely, the methane, R134a, R410a, and R507a at temperatures ranging from (5 to 45) °C.

Impact on Gaseous Compressibility. To understand the gaseous transport mechanism in the pitch-based activated carbon micropores and extract the transport parameters from the experimental uptake results, it is necessary to quantify the effect of temperature changes due to the sudden compression (pressurization) of adsorbate into the sorption cylinder.

The effect was measured by conducting "blank runs" (without any adsorbent in the test chamber) at respective conditions similar to the actual experiments. The actual temperature effects due to adsorption, that is, heat of adsorption can then be determined by offsetting the temperature increase during the "blank runs" with the temperatures rise measured from the kinetics experiments.

RESULTS AND DISCUSSION

In this work, the experimentally measured kinetics data for the adsorption of methane, refrigerant R-134a, R-410a (near azeotropic blend of HFC-32 and HFC-125), and R-507a (azeotropic blend of HFC-125 and HFC-143a) onto pitch-based carbonaceous material (Maxsorb III) are correlated with the proposed nonisothermal kinetics model. The kinetics tests are conducted at four different set temperatures ((5, 15, 30, and 45) °C) and pressures up to 10 bar.

Effects of Heat Evolution during Adsorption Process. At first, the adsorbent temperatures rose during the kinetics experiment are present in Figure 5. The graphs show the adsorbent temperature profiles in current experiments during the adsorption process for refrigerants R134a, R410a, R507a, and methane onto Maxsorb III at the respective pressures and temperatures. In contrast, the charging chamber temperatures remained constant throughout the experiment. With the initial temperatures for all four cases maintained at preselected conditions, the adsorbent temperature rose drastically and reached its peak within 20 s during the adsorption process. These are consistent with adsorption as an exothermic process; that is, thermal energy (isosteric heat of adsorption) is released during adsorption. In all cases, the adsorbent experienced a significant temperature increase, that is, more than two times of the initial equilibrium temperature. The increases in adsorbent temperature are more significant in adsorption of halocarbon refrigerants compared with methane adsorption onto Maxsorb III. With these results, it is concluded that the effect of adsorbent temperatures is important in the analysis of kinetics gas adsorption mechanism. Therefore, it is vital that a nonisothermal kinetics model is required to predict the actual kinetics behavior of the vapor uptake, as proposed in eq 15.

During the kinetics experiment, the adsorption cell was submerged in a temperature-controlled water circulator to maintain the adsorbent at equilibrium temperature. Hence, the adsorbent eventually reached the equilibrium temperature. The adsorption process was continued until the system pressures and temperatures became stabilized, at which the rate of change for pressure and temperature are less than 1 mbar/30 min and 0.2 °C/30 min, respectively.

On the other hand, Figure 6 illustrates both the pressure profiles in the adsorption and charging chambers for Maxsorb III-R134a at P^* = 3.1 bar, T^* = 5 °C. The adsorption cell pressure was maintained constant throughout the kinetics process using the electronic-controlled pressure regulator to study the kinetics mechanism in constant concentration conditions. The adsorption cell pressure reached its preset pressure within (2 to 3) s from the instant that the regulator is opened.

Effects of Compressibility of Adsorbate during Charging. Furthermore, to understand the exact gaseous transport mechanism in the single component adsorbent−adsorbate systems (i.e., Maxsorb III-CH_4, Maxsorb III-R134a and Maxsorb III-R507a) it is necessary to quantify the effects of temperature changes due to the sudden compression (pressurization) of adsorbate into the sorption cylinder. Hence the temperature increases due to sudden compression were measured by conducting "blank runs" experiment, that is, with no specimens inside the sorption cell, at respective conditions similar to the actual kinetics experiments. Figure 7 shows the temperature profiles of the kinetics tests, the "blank runs", and the offset temperatures for refrigerant R134a with Maxsorb III at an equilibrium pressure and temperature of 3.1 bar and 5 °C, respectively. The offset temperature is simply calculated by the following equation,

$$T_{\text{offset}} = T_{\text{ads}} - (T_{\text{empty}} - T^*) \tag{16}$$

where T_{ads} represents the adsorbent temperature during the kinetics tests and T_{empty} is the sorption cell temperature during the blank runs.

The percentage deviations for the kinetics results for the actual run and "blank run" are shown in Figure 8. It is noticed that the effects of temperature change in the sorption cell during the blank runs are insignificant for pressures lower than 10 bar; that is, the uptake deviations are less than 3 %. Hence in the current analysis, the effect of temperature rise due to sudden pressurization of adsorbate is neglected. However, for higher adsorption pressures, that is, greater than 10 bar, necessary precautions need to be considered for the sudden compression of the adsorbate which may lead to considerable temperature increase in the system.

Validation of Proposed Model with Experimental Kinetics Data. The experimental adsorption uptakes for refrigerant R134a with activated carbon Maxsorb III at (5, 15, 30, 45, and 60) °C are plotted with respect to time in Figure 9. The equilibrium pressures for the kinetics experiment are selected to be lowered than the saturation pressure at their respective temperatures. This is to prevent any possible condensation of adsorbate in the chambers. As shown in Figure 9a, the kinetics tests are conducted at only two sets of equilibrium pressures, that is, (1.1 and 2.1) bar. Meanwhile, at higher system temperatures, the kinetics tests are conducted for pressures setting up to 5.1 bar, that is, for system temperatures of (30, 45, and 60) °C.

It may be observed that there is a sudden increase in uptake values at the very beginning of the kinetics test and, especially for higher system pressures, the effects are more significant. The uptakes are then slowly reduced and eventually increased again to reach its equilibrium uptake values. The possible explanation for the phenomenon is that the sudden increases of uptake values are mainly due to the sudden charging of the adsorbate into the sorption cell at higher pressures; that is, the adsorbate molecules "rush" into the sorption cell and are adsorbed onto the solid adsorbent surfaces. However, this will cause the evolution of isosteric heat of adsorption which leads to the increase in adsorbent temperature. The adsorbed refrigerant molecules are desorbed due to the temperature increased; that is, uptake values decrease gradually. Since during the kinetics test, the external heat sink is rejecting the isosteric heat of adsorption, and the adsorbent ultimately reaches the predetermined temperature; that is, the temperature of the adsorbent decreases, and hence the adsorption of refrigerant increases and reaches the equilibrium uptake. This shows the importance of thermal management in any solid sorption systems, either to reject the isosteric heat of adsorption or supply heat during desorption processes.

The proposed nonisothermal kinetics model and dotted lines are also plotted in Figure 9 to predict the kinetics values. This model which incorporated the system pressures and adsorbent temperatures effects gives a satisfactory approximation to the adsorption uptake behavior.

The average regression error of the proposed model for adsorbent−adsorbate pairs (Maxsorb III-R134a, Maxsorb III-R410a, Maxsorb III-R507a, and Maxsorb III-CH_4) are shown in Figure 10, which are less than 8.5 %.

The kinetics experiment data for Maxsorb III-R410a, Maxsorb III-R507a, and Maxsorb III-CH_4 can be found in Figures 11 to 13, respectively. The proposed correlations are also superimposed onto the graphs.

The pre-exponential function D^*_{so}, which is a function of equilibrium pressure, P^* (eq 10) for Maxsorb III-R134a, Maxsorb III-R410a, Maxsorb III-R507a, and Maxsorb III-CH_4 are plotted against the pressure ratio, P^*/P_{cri}, as shown in Figure 14. The pre-exponential function D^*_{so} shows an increasing trend with increasing equilibrium pressure, for the Maxsorb III with the halocarbon refrigerants. Conversely it shows a decreasing trend with increasing system pressure for the Maxsorb III-CH_4 pair. The values of D^*_{so} are between 0.1 and 0.8. The coefficients (A_1 and A_2) of the pre-exponential function D^*_{so} are presented in Table 2.

With these regressed values, the effective mass transfer coefficients k_sa_v of Maxsorb III-R134a, Maxsorb III-R410a, Maxsorb III-R507a, and Maxsorb III-methane are plotted against the pressure ratio, P^*/P_{cri} at respective temperatures, that is, (5, 15, 30, 45, and 60) °C, in Figure 15. The effective mass transfer coefficients, k_sa_v, increase with increasing system temperatures. In addition, the k_sa_v have the same trends as the D^*_{so}, that is, increasing with increasing in equilibrium pressure, for Maxsorb III with halocarbon refrigerant, while decreasing with increasing in system pressure for Maxsorb III-CH_4 pair.

This dissimilarity is due to the difference in adsorption temperatures; that is, the CH_4 operate above the critical temperature, whereas the others operate below the critical temperature of the adsorbates. The similar decreasing trends of k_sa_v with system pressures of hydrocarbons can be found in a previous work by Ruthven and Derrah, at which the system temperatures are below the critical temperature and the k_sa_v also increase with increasing system temperatures.[39]

On the other hand, the temperature-dependent effective mass transfer coefficients, β for all four working pairs, are plotted against the temperature ratio, T^*/T in Figure 16. The β values are found to be increasing with the system temperatures for all cases studied, with values between (0.25 and 0.9) s^{-1}. The coefficients (B_1 and B_2) of β for all four adsorbent−adsorbate pairs are presented in Table 2.

CONCLUSIONS

The kinetics experiment data for Maxsorb III-R134a, Maxsorb III-R410a, Maxsorb III-R507a, and Maxsorb III-CH_4 are successfully obtained and correlated using the proposed nonisothermal kinetics equation. The parameters derived from the model are consistent, reproducible, and agree well with a priori estimates. The average regression error of the proposed model for adsorbent−adsorbate pairs (Maxsorb III-R134a, Maxsorb III-R410a, Maxsorb III-R507a, and Maxsorb III-CH_4) are less than 8.5 %. The model provides a useful theoretical basic for the analysis of rapid sorption processes for which the isothermal approximation is no longer valid.

AUTHOR INFORMATION

Corresponding Author

*Phone: +65 65162214. Fax: +65-6779-1459. E-mail: mpengkc@nus.edu.sg.

Notes

The authors declare no competing financial interest.

Funding

This work was supported by the Singapore Agency for Science, Technology and Research (A*STAR) and the Singapore Maritime and Port Authority (MPA) under grant number R265-000-268-305/490.

REFERENCES

(1) Glueckauf, E. Theory of chromatography part 10: Formula for diffusion into spheres and their applications in chromatography. *Trans. Faraday Soc.* **1955**, *51*, 1540−1551.

(2) Guilleminot, J. J.; Choisier, A.; Chalfen, J. B.; Nicolas, S.; Reymoney, J. L. Heat transfer intensification in fixed bed adsobers. *Heat Recovery Syst. CHP* **1993**, *13*, 297−300.

(3) Lathan, J. L.; Burgess, A. E. *Elementary Reaction Kinetics*; Butterworths: London, 1981; pp 13−24.

(4) Sircar, S.; Hufton, J. R. Intraparticle adsorbate concentration profile for linear driving force model. *AIChE J.* **2000**, *46*, 659−660.

(5) Li, Z.; Yang, R. T. Concentration profile for linear driving force model for diffusion in a particle. *AIChE J.* **1999**, *45*, 196−200.

(6) Fletcher, A. J.; Thomas, K. M. Adsorption and desorption kinetics of n-octane and n-nonane vapors on activated carbon. *Langmuir* **1999**, *15*, 6908−6914.

(7) Fletcher, A. J.; Yüzak, Y.; Thomas, K. M. Adsorption and desorption kinetics for hydrophilic and hydrophobic vapors on activated carbon. *Carbon* **2006**, *44*, 989−1004.
(8) Malek, A.; Farooq, S. Kinetics of hydrocarbon adsorption on activated carbon and silica gel. *AIChE J.* **1997**, *43*, 761−776.
(9) Scholl, S.; Kajszika, H.; Mersmann, A. Adsorption and desorption kinetics in activated carbon. *Gas Sep. Purif.* **1993**, *4*, 207−212.
(10) El-Sharkawy, I. I.; Saha, B. B.; Koyama, S.; Ng, K. C. A study on the kinetics of ethanol-activated carbon fiber: theory and experiments. *Int. Heat Mass Transfer* **2006**, *49*, 3104−3110.
(11) Saha, B. B.; El-Sharkawy, I. I.; Chakraborty, A.; Koyama, S.; Yoon, S. H.; Ng, K. C. Adsorption rate of ethanol on activated carbon fiber. *J. Chem. Eng. Data* **2006**, *51*, 1587−1592.
(12) Reid, C. R.; Thomas, K. M. Adsorption of gases on a carbon molecular sieve used for air separation: linear adsorptives as probes for kinetics selectivity. *Langmuir* **1999**, *15*, 3206−3218.
(13) Reid, C. R.; O'Koye, I. P.; Thomas, K. M. Adsorption of gases on carbon molecular sieves used for air separation: spherical adsorptives as probes for kinetics selectivity. *Langmuir* **1998**, *14*, 2415−2425.
(14) Harding, A. W.; Foley, N. J.; Norman, P. R.; Francis, D. C.; Thomas, K. M. Diffusion barriers in the kinetics of water vapor adsorption/desorption on activated carbons. *Langmuir* **1998**, *14*, 3858−3864.
(15) Crank, J. *The Mathematics of Diffusion*; Oxford University Press: London, 1956, 56.
(16) Chihara, K.; Suzuki, M.; Kawazoe, K. Effect of heat generation on measurement of adsorption rate by gravitatric method. *Chem. Eng. Sci.* **1976**, *31*, 505−507.
(17) Sircar, S. On the measurement of sorption kinetics by differential test: Effect of the heat of sorption. *Carbon* **1981**, *19* (4), 285−288.
(18) Eagan, J. D.; Kindl, B.; Anderson, R. B. *Molecular Sieve Zeolites-II*; American Chemical Society: Washington, DC, 1971; Chap. 52, Vol. *102*; pp 164−170.
(19) Doelle, H. J.; Riekert, L. Kinetics of sorption, desorption, and diffusion of n-butane in zeolite NaX. *ACS Symp. Ser.* **1977**, *40*, 401−416.
(20) Ilavský, J.; Brunovská, A.; Hlaváček, V. Experimental observation of temperature gradient occurring in a single zeolite pallet. *Chem. Eng. Sci.* **1980**, *35*, 2475−2479.
(21) Voloshchuk, A. M.; Dubinin, M. M.; Erashko, I. T.; Bezus, A. G.; Zikanova, A.; Kocirik, M. Kinetics of nonisothermal adsorption by biporous adsorbents. Communication 4. Kinetics of Cyclohexane adsorption by NaX Zeolite. *Izv. Akad. Nauk SSSR, Ser. Khim.* **1983**, *10*, 2192−2198.
(22) Voloshchuk, A. M.; Gorlov, V. A.; Dubinin, M. M.; Erashko, I. T.; Broddak, R. Kinetics of nonisothermal adsorption by biporous adsorbents. Communication 1. Effect of finite rate of dissipation of heat of adsorption on kinetics of adsorption by Zeolites. *Izv. Akad. Nauk SSSR, Ser. Khim.* **1983**, *7*, 1463−1468.
(23) Voloshchuk, A. M.; Gorlov, V. A.; Dubinin, M. M.; Erashko, I. T.; Zolotarev, P. P.; Ugrozov, V. V. Kinetics of nonisothermal adsorption by biporous adsorbents. Communication 3. Kinetics of the adsorption of Xenon by CaA Zeolite. *Izv. Akad. Nauk SSSR, Ser. Khim.* **1983**, *8*, 1710−1715.
(24) Fiani, E.; Perier-Cambry, L.; Thomas, G. Non-isothermal modeling of hrydrocarbon adsorption on a granulated active carbon. *J. Therm. Anal. Calorim.* **2000**, *60*, 557−570.
(25) Meunier, F.; Sun, L. M.; Kraehenbuehl, F.; Stoeckli, F. A comparison of experimental and theoretical adsorption kinetics of dichloromethane vapour by active carbon under non-isothermal conditions. *J. Chem. Soc., Faraday Trans. I* **1998**, *84* (6), 1973−1983.
(26) Brunovská, A.; Hlaváček, V.; Ilavský, J.; Valtýni, J. An analysis of a nonisothermal one-component sorption in a single adsorbent particle. *Chem. Eng. Sci.* **1978**, *33*, 1385−1391.
(27) Brunovská, A.; Hlaváček, V.; Ilavský, J.; Valtýni, J. Non-isothermal one-component sorption in a single adsorbent particle. Effect of external heat transfer. *Chem. Eng. Sci.* **1980**, *35*, 757−759.
(28) Brunovská, A.; Ilavský, J.; Hlaváček, V. An analysis of a nonisothermal one-component sorption in a single adsorbent particle-a simplified model. *Chem. Eng. Sci.* **1981**, *36*, 123−128.
(29) Zolotarev, P. P. The kinetics of nonisothermal adsorption. *Izv. Akad. Nauk SSSR, Ser. Khim.* **1970**, *6*, 1421−1423.
(30) Zolotarev, P. P. Theory of the kinetics of adsorption taking into account heat evolution, where the rate of the process is limited by external mass and heat transfer. *Izv. Akad. Nauk SSSR, Ser. Khim.* **1970**, *12*, 2831−2833.
(31) Sircar, S. Linear-driving-force model for non-isothermal gas adsorption kinetics. *J. Chem. Soc., Faraday Trans. I* **1983**, *79*, 785−796.
(32) Armstrong, A. A.; Stannett, V. Temperature effects during the sorption and desorption of water vapor in high polymers. I. Fibers with particular reference to wool. *Makromol. Chem.* **1966**, *90*, 145−160.
(33) Ruthven, D. M.; Lee, K. L.; Yuccel, J. Kinetics of non-isothermal sorption in molecular sieve crystals. *AIChE J.* **1980**, *26* (1), 16−23.
(34) Ruthven, D. M.; Lee, K. Kinetics of nonisothermal sorption: Systems with bed diffusion control. *AIChE J.* **1981**, *27* (4), 654−663.
(35) Lee, K. L.; Ruthven, D. M. Analysis of thermal effects in adsorption rate measurements. *J. Chem. Soc., Faraday Trans. I* **1979**, *75*, 2406−2422.
(36) Kocirik, M.; Smutek, M.; Bezus, A.; Zikanova, A. Analysis of adsorption kinetics on zeolites under nonisothermal conditions. I. Analytical solution of the problem. *Collect. Czech. Chem. Commun.* **1980**, *45* (12), 3392.
(37) He, J. M.; Ng, K. C.; Yap, C.; Saha, B. B. Effect of pressure on the adsorption rate for gasoline vapor on pitch-based activated carbon. *J. Chem. Eng. Data* **2009**, *54*, 1504−1509.
(38) Belmabkhout, Y.; Frere, M.; Weireld, G. D. High-pressure adsorption measurements. A comparative study of the volumetric and gravimetric methods. *Measure. Sci. Technol.* **2005**, *15*, 848−858.
(39) Ruthven, D. M.; Derrah, R. I. Sorption in Davison 5A molecular sieves. *Can. J. Chem. Eng.* **1972**, *50*, 743−747.